HOKKAIDO UNIVERSITY

| | |
|---|---|
| Title | Polyethylene glycol promotes autoxidation of cytochrome c |
| Author(s) | Sato, Wataru; Uchida, Takeshi; Saio, Tomohide; Ishimori, Koichiro |
| Citation | Biochimica et Biophysica Acta (BBA) - General Subjects, 1862(6), 1339-1349<br>https://doi.org/10.1016/j.bbagen.2018.03.010 |
| Issue Date | 2018-06 |
| Doc URL | http://hdl.handle.net/2115/72937 |
| Rights | © 2018. This manuscript version is made available under the CC-BY-NC-ND 4.0 license<br>http://creativecommons.org/licenses/by-nc-nd/4.0/ |
| Rights(URL) | http://creativecommons.org/licenses/by-nc-nd/4.0/ |
| Type | article (author version) |
| File Information | j.bbagen.2018.03.010-HUSCAP.pdf |

Instructions for use

Hokkaido University Collection of Scholarly and Academic Papers : HUSCAP

Accepted Manuscript


# Polyethylene glycol promotes autoxidation of cytochrome c

Wataru Sato, Takeshi Uchida, Tomohide Saio, Koichiro Ishimori

PII: S0304-4165(18)30072-2
DOI: doi:10.1016/j.bbagen.2018.03.010
Reference: BBAGEN 29061

To appear in:

Received date: 10 October 2017
Revised date: 5 March 2018
Accepted date: 8 March 2018

Please cite this article as: Wataru Sato, Takeshi Uchida, Tomohide Saio, Koichiro Ishimori , Polyethylene glycol promotes autoxidation of cytochrome c. The address for the corresponding author was captured as affiliation for all authors. Please check if appropriate. Bbagen(2018), doi:10.1016/j.bbagen.2018.03.010

This is a PDF file of an unedited manuscript that has been accepted for publication. As a service to our customers we are providing this early version of the manuscript. The manuscript will undergo copyediting, typesetting, and review of the resulting proof before it is published in its final form. Please note that during the production process errors may be discovered which could affect the content, and all legal disclaimers that apply to the journal pertain.

ACCEPTED MANUSCRIPT

# Polyethylene glycol promotes autoxidation of cytochrome *c*

Wataru Sato[1], Takeshi Uchida*[1,2], Tomohide Saio[1,2,3], and Koichiro Ishimori*[1,2]

[1]Graduate School of Chemical Sciences and Engineering, Hokkaido University, Sapporo 060-8628, Japan

[2]Department of Chemistry, Faculty of Science, Hokkaido University, Sapporo 060-0810, Japan

[3]PRESTO, Japan Science and Technology Agency, Sapporo 060-0810, Japan

ACCEPTED MANUSCRIPT

ACCEPTED MANUSCRIPT

**ABSTRACT**

Cytochrome *c* (Cyt *c*) was rapidly oxidized by molecular oxygen in the presence, but not absence of PEG. The redox potential of heme *c* was determined by the potentiometric titration to be +236 ± 3 mV in the absence of PEG, which was negatively shifted to +200 ± 4 mV in the presence of PEG. The underlying the rapid oxidation was explored by examining the structural changes in Cyt *c* in the presence of PEG using UV-visible absorption, circular dichroism, resonance Raman, and fluorescence spectroscopies. These spectroscopic analyses suggested that heme oxidation was induced by a modest tertiary structural change accompanied by a slight shift in the heme position (<1.0 Å) rather than by partial denaturation, as is observed in the presence of cardiolipin. The near-infrared spectra showed that PEG induced dehydration from Cyt *c*, which triggered heme displacement. The primary dehydration site was estimated to be around surface-exposed hydrophobic residues near the heme center: Ile81 and Val83. These findings and our previous studies, which showed that hydrated water molecules around Ile81 and Val83 are expelled when Cyt *c* forms a complex with C*c*O, proposed that dehydration of these residues is functionally significant to electron transfer from Cyt *c* to C*c*O.

Keywords: heme; cytochrome c; electron transfer; dehydration

ACCEPTED MANUSCRIPT

ACCEPTED MANUSCRIPT

## 1. Introduction

Electron transfer (ET) reactions in mitochondrial and bacterial respiratory chains are essential for energy transduction in cells. A series of ET steps in respiratory chain reactions are terminated at cytochrome *c* oxidase (C*c*O), where molecular oxygen is reduced to water. Coupled to molecular oxygen reduction, C*c*O functions as a proton pump across the mitochondrial inner membrane, and the resulting proton gradient is a primary driving force for ATP synthesis [1–3]. In C*c*O, electrons that reduce molecular oxygen are donated from a small water-soluble hemoprotein, cytochrome *c* (Cyt *c*). Cyt *c* carries one electron to C*c*O and has been proposed to specifically interact with C*c*O to form an ET complex, which promotes ET from the heme iron in Cyt *c* to $Cu_A$ in C*c*O [4–10].

Over the past few decades, extensive research has led to considerable improvements in our understanding of the interaction between Cyt *c* and C*c*O. Studies have demonstrated the involvement of electrostatic interactions mediated by lysine residues surrounding the heme edge in Cyt *c* and acidic residues around $Cu_A$ in C*c*O [4–8]. The dependence of the ET rate on the ionic strength supports the significant contributions of the electrostatic interactions to the formation of the ET complex [9,10]; however, NMR analysis of the human Cyt *c*-bovine C*c*O complex identified several hydrophobic residues, including Ile9, Ile11, Met12, Cys17, and Ile81, that contribute to the formation of the ET complex [11]. An NMR analysis of the interaction sites and the mutational effects on the steady-state kinetics of the ET reaction were used to design docking simulations that provided the structure of the ET complex between human Cyt *c* and bovine C*c*O [12]. The predicted Cyt *c*-C*c*O ET complex suggested that hydrophobic interactions, rather than electrostatic interactions, were the primary thermodynamic factor that stabilized complex formation. Favorable (Columbic) electrostatic interactions between several charged residues were nearly cancelled out by large unfavorable (desolvation) electrostatic interactions. Jelesarov et al. also pointed out the importance of hydrophobic interactions for association of other electron carrier protein, ferredoxin, with

ACCEPTED MANUSCRIPT

ferredoxin:$NADP^+$ reductase by isothermal titration calorimetry [13].

These previous studies were carried out under "simplified" conditions, in which the isolated proteins were modeled and all other macromolecular species were absent. Because the cell interior is a heterogeneous crowded solution of proteins, nucleic acids, small molecules, and lipid bilayer membranes, the cytoplasm contains up to 400 g $L^{-1}$ macromolecules occupying 5–40% of the total volume of the cell [14]. Especially, recent studies suggest that high concentration of several macromolecules can affect the nature of water hydration, altering the dielectric constant and, in turn, affecting the structures, dynamics, and functions of proteins [15,16], facilitating ligand binding and formation of protein–protein complexes through excluded volume effects [17–21]. In the case of human Cyt *c* and bovine C*c*O, however, the influence of alteration of the hydration environment by macromolecules on the formation of protein–protein complexes remain unclear.

One of the useful approaches to form an environment with low dielectric constant, *i.e.* more hydrophobic environment, in an aqueous solvent involves the use of synthetic cosolutes, polyethylene glycol (PEG). High concentrations of PEG are known to cause dehydration from the surfaces of proteins and often used to protein precipitation [22–24].

Detailed experimental characterizations of the mechanism underlying Cyt *c*-C*c*O ET complexation under physiological conditions have been quite limited. Here, we describe a study of the influence of PEG 4000, on the structure and function of Cyt *c*. Unexpectedly, we found that the heme iron in Cyt *c* was rapidly oxidized in the presence of PEG. Spectroscopic measurements suggested that oxidation of the heme iron was induced by a slight tertiary structural change accompanied by the displacement of the heme, rather than by partial denaturation of Cyt *c*. Site-directed mutagenesis clearly revealed that heme displacement in the presence of PEG was triggered by dehydration of the surface-exposed hydrophobic region near the heme. These results suggested that the PEG-induced change in the hydration structure around the surface of Cyt *c* produced a conformational change. We explored the

ACCEPTED MANUSCRIPT

contribution of dehydration from the hydrophobic region around the surface-exposed heme periphery to ET to C*c*O in terms of the heme's redox potential.

## 2. Materials and methods

### *2.1. Protein expression and purification*

Native and $^{15}$N-labeled human Cyt *c* were expressed in *Escherichia coli* and purified as previously described [11,12]. Briefly, Rosetta2(DE3)pLysS (Novagen, Madison, WI) cells transformed with the plasmids containing human Cyt *c* [25] DNA were inoculated in 5 mL 2xYT medium and grown overnight. This pre-cultured medium was added to 1 liter 2xYT or M9 medium containing $^{15}$N-ammonium chloride, and the bacteria were further incubated at 37°C. The expression of Cyt *c* was initiated by adding 0.8 mM isopropyl 1-thio-β-D-galactopyranoside to the culture when the optical density at 600 nm reached 0.6. Then, 0.1 mM δ-aminolevulinic acid was added to promote heme biosynthesis. After incubation for an additional 24 h in the 2xYT medium or 72 h in the M9 medium, the cells were harvested by centrifugation.

The cell pellet was resuspended in 50 mM Tris-HCl (pH 7.5) containing 1 g $L^{-1}$ lysozyme, 50 mg $L^{-1}$ DNase I, and 50 mg $L^{-1}$ RNase A and suspended for 3 h to lyse the cell pellet completely. The supernatant of the crude extract was obtained by centrifugation at 18,000 rpm for 5 min and 40,000 rpm for 1 h. The supernatant was purified using a HiPrep 16/10 SP XL column (GE Healthcare, Uppsala, Sweden) with a linear salt gradient of 1–300 mM NaCl. The elution sample was concentrated by Amicon ultrafiltration using 5 kDa cutoff membranes. The concentrated Cyt *c* was a mixture of ferric and ferrous forms, so the Cyt *c* was stirred in a 10× potassium ferricyanide solution for 1 h. After dissolving in a 50 mM sodium phosphate buffer (pH 7.0), Cyt *c* was further purified using a Mono S 10/100 GL column (GE

ACCEPTED MANUSCRIPT

Healthcare) with a linear salt gradient of 1–300 mM NaCl. The purified Cyt *c* fractions were pooled, concentrated, and applied to a HiLoad 16/60 Superdex 75 gel filtration column (GE Healthcare).

*2.2. Site-directed mutagenesis*

Mutagenesis was conducted utilizing a PrimeSTAR mutagenesis basal kit from Takara Bio (Otsu, Japan). DNA oligonucleotides were purchased from Eurofins Genomics (Tokyo, Japan). The mutated genes were sequenced to ensure that only the desired mutations were introduced (Eurofins Genomics).

*2.3. Ferrous Cyt c autoxidation kinetics*

The ferrous Cyt *c* autoxidation kinetics were studied using a Hitachi U-3310 UV-visible spectrophotometer (Tokyo, Japan) at 293 K in a 50 mM sodium phosphate buffer (pH 7.0). Ferrous Cyt *c* was prepared by reducing ferric Cyt *c* with sodium dithionite, and excess reductant was removed using a PD MiniTrap G-25 column (GE Healthcare). The concentration of PEG 4000 or trehalose (Wako Pure Chemical Industries, Osaka, Japan) was varied between 0 and 20%. Oxidation of Cyt *c* was monitored by measuring the absorbance at 550 nm after adding ferrous Cyt *c* to the reaction solution at a final concentration of 3 μM. The absorption at 550 nm was recorded in intervals of 0.5 s over 5 min. The end point of Cyt *c* autoxidation was determined by adding a small amount of potassium ferricyanide to the reaction solution.

*2.4. Absorption spectroscopy*

ACCEPTED MANUSCRIPT

The absorption spectra were collected using a Hitachi U-3310 UV-visible spectrophotometer from solutions prepared at 293 K in 50 mM sodium phosphate buffer (pH 7.0). Spectra were recorded between 250 and 700 nm or 600 and 800 nm in intervals of 1 nm or 0.2 nm, respectively. The PEG 4000 concentration was varied between 0 and 20%, and the Cyt *c* concentration was 8 μM (for the 250–700 nm measurement) or 0.3 mM (for the 600–800 nm measurement).

*2.5. Circular dichroism spectroscopy*

Circular dichroism (CD) spectra were recorded using a JASCO J-1500 CD spectrometer (Tokyo, Japan) with 10 mm path length cuvettes at room temperature in 50 mM sodium phosphate buffer (pH 7.0). Each spectrum represented the integration of three consecutive scans from 390 to 440 nm or from 190 to 250 nm at 0.2 nm intervals, with a scan speed of 20 nm/min. The spectrum bandwidth was fixed at 1.0 nm. The PEG 4000 concentration was varied between 0 and 20%, and the Cyt *c* concentration was 10 μM for measurement of the Soret region or 2 μM for measurement of the far-UV region. The ellipticity was expressed as the mean residue molar ellipticity (deg $cm^2$ $dmol^{-1}$), calculated using the JASCO software.

*2.6. Resonance Raman spectroscopy*

Resonance Raman spectra were recorded using a single monochrometer (SPEX500M, Jobin Yvon, Edison, NJ) equipped with a liquid nitrogen-cooled CCD detector (Spec-10:400B/LN, Roper Scientific, Princeton, NJ). Samples were excited at a wavelength of 441.6 nm delivered by a helium-cadmium laser (IK5651R, Kimmon Koha, Tokyo, Japan). The laser power at the sample point was adjusted to 5 mW. Raman shifts were calibrated using indene and $CCl_4$. The accuracy of the well-defined Raman band peak positions was ± 1

ACCEPTED MANUSCRIPT

$cm^{-1}$. The PEG 4000 concentration was varied between 0 and 5%, and the Cyt *c* concentration was 50 μM.

*2.7. Fluorescence spectroscopy*

Fluorescence measurements were collected using a JASCO FP-8500 spectrofluorometer from solutions prepared at 293 K in 50 mM sodium phosphate buffer (pH 7.0). Unpolarized emission spectra were recorded between 300 and 450 nm using a 280 nm excitation wavelength and a scan speed of 200 nm/min. The excitation and emission slit widths were 5 and 10 nm, respectively. Each spectrum represents the integration of three consecutive scans. The measurements were carried out in the absence or presence of 6 μM Cyt *c* with 0, 5, or 10% PEG, and the spectra of the PEG solution were subtracted from the spectra of the Cyt *c*-containing solution.

*2.8. Near-infrared spectroscopy*

Near-infrared spectra were recorded using a JASCO V-570 spectrometer with a 1 mm path length cuvette, using solutions prepared at room temperature in 50 mM sodium phosphate buffer (pH 7.0). Each spectrum represents the integration of three consecutive scans from 1300 to 1600 nm in 0.2 nm intervals, with a scan speed of 200 nm/min. The spectral bandwidth was fixed at 2.0 nm. The measurements were carried out in the absence or presence of 50 μM Cyt *c* and 0, 5, or 10% PEG, and the spectra of the PEG solutions were subtracted from the spectra of the Cyt *c*-containing solutions.

*2.9. NMR spectroscopy*

ACCEPTED MANUSCRIPT

$^{1}$H-$^{15}$N HSQC NMR measurements were performed at 293 K using a Bruker AVANCE III HD 600 MHz spectrometer. All spectrum were processed by NMRpipe [26], and the data were analyzed using SPARKY. In the $^{1}$H-$^{15}$N HSQC experiments, each sample contained 0.15 mM oxidized Cyt *c* and 5% $D_2O$ in a 50 mM sodium phosphate buffer (pH 7.0). $^{15}$N-labeled Cyt *c* was studied in the presence of 20% PEG. $^{1}$H-$^{15}$N HSQC spectra were collected using the spectral widths 16 ppm and 38 ppm for the $^{1}$H and $^{15}$N dimensions, respectively, and 2048 and 300 complex points were set for the $^{1}$H and $^{15}$N dimensions, respectively [11].

After identifying the amide signals based on sequential assignments and peak fits using SPARKY, the PEG-induced changes in the backbone amide proton and nitrogen chemical shifts in Cyt *c* were determined. $^{1}$H and $^{15}$N chemical shifts were combined using the following equation [27] to calculate the composite chemical shifts.

$$\Delta\delta_{NH}=\left\{\Delta\delta_{H}^{2}+(\Delta\delta_{N}/6.5)^{2}\right\}^{1/2}, \quad (1)$$

All NMR samples used for the $^{1}$H measurements contained 0.15 mM oxidized Cyt *c*, 10 or 20% PEG and 5% $D_2O$ in 50 mM sodium phosphate buffer (pH 7.0). $^{1}$H NMR measurements were performed using an Agilent Unity INOVA 600 spectrometer. Chemical shifts were referenced to the signals obtained from 4,4-dimethyl-4-silapentane-1-sulfonic acid (DSS). A series of $^{1}$H NMR experiments was performed using a presaturation pulse program with a spectral width of 80 ppm. Significant signals from PEG were suppressed by adding a WURST-2 pulse 2 ppm wide and centered at 4.23 ppm.

*2.10. Potentiometric titration*

Potentiometric titrations were performed in an anaerobic cuvette at 293 K with continuous flow of humidified nitrogen gas. A three-electrode configuration of consisted of a platinum wire meshes as a working electrode, a platinum wire meshes as a counter electrode, and

ACCEPTED MANUSCRIPT

saturated Ag/AgCl electrode as a reference electrode. The potentials of these electrodes were controlled by a Hokuto Denko HSV-110 potentiostat/galvanostat (Tokyo, Japan). Samples (0.4 mL) containing 40 μM Cyt *c* in 50 mM sodium phosphate buffer (pH 7.0) were used. Electrode-solution mediation was facilitated by the following mediators: 15 μM *N*,*N*-dimethyl-*p*-phenylendiamine ($E_m$ = +340 mV), 20 μM *N*,*N*,*N*′,*N*′-tetramethyl-*p*-phenylendiamine ($E_m$ = +260 mV), 15 μM 2,6-dichlorophenolindophenol ($E_m$ = +217 mV), 50 μM 1,2-naphtoquinone ($E_m$ = +145 mV), phenazine methosulfate ($E_m$ = +80 mV), 15 μM gallocyanine ($E_m$ = +20 mV), 15 μM indigo trisulfonate ($E_m$ = –80 mV), 15 μM 2-hydroxy-1,4-napththoquinone ($E_m$ = –120 mV), and 10 μM anthraquinone-2-sulfonic acid ($E_m$ = –230 mV). Absorption spectra were recorded from 350 to 700 nm using a Hitachi U-3310 UV-visible spectrophotometer equipped with a Peltier-type temperature control system. The potential of electrode was decrease in 50 mV steps until the protein was fully reduced and increased stepwise until reoxidation was complete. The ratio of reduced heme was calculated by deconvoluting each absorption spectrum into two components—an absorption spectrum at –100 mV (defined as 100% reduced heme) and one at 500 mV (defined as 100% oxidized heme) Heme reduction was monitored by the increase in the α-band absorption at 550 nm, where the absorption of the mediators was negligible compared to that of the protein. Potential values were described relative to the normal hydrogen electrode (NHE) by adding 197 mV to the imposed potentials. The titration data were analyzed by fitting with the Nernst equation for a single-electron process.

## 3. Results

### *3.1. Electron transfer from Cyt c in the presence of PEG*

ACCEPTED MANUSCRIPT

We investigated whether the oxidation rate of the human Cyt *c* heme iron increased upon the addition of PEG 4000 by measuring the apparent oxidation rate of Cyt *c* in the presence of PEG. This was achieved by monitoring the absorbance at 550 nm. The absorbance at 550 nm of Cyt *c* decreased over time in the presence of PEG (Figure 1), whereas the absorbance at 550 nm in the absence of PEG remained constant over 1 week. By contrast, Cyt *c* was not oxidized in the absence and presence of PEG under anaerobic condition, indicating that the heme of Cyt *c* was oxidized by molecular oxygen ($O_2$) only in the presence of PEG. To estimate the apparent oxidation rate of reduced Cyt *c* by $O_2$, $k_{app}$, the absorbance change at 550 nm measured at 1 s intervals over 300 s was fit to the following equation:

$$\mathrm{Abs}_{550}(t) = A\exp\left(-k_{\mathrm{app}}t\right) + B, \qquad (2)$$

where $\mathrm{Abs}_{550}(t)$ is the absorbance at 550 nm as a function of time, $A$ is a constant related to the initial absorbance, and $B$ is the final absorbance, respectively. The $k_{app}$ in the presence of 10% PEG was estimated to be $0.0031 \pm 0.0001$ $s^{-1}$ using equation 2. These results indicated that Cyt *c* was oxidized almost completely within approximately 20 min. These results suggested that PEG significantly promoted electron flow from Cyt *c* to molecular oxygen, leading to oxidation of the Cyt *c* heme.

*3.2. Structural properties of Cyt c in the presence of PEG*

The driving force underlying the rapid oxidation of Cyt *c* in the presence of PEG was investigated by first considering the possibility that PEG partially denatured Cyt *c*. Figure 2A plots the absorption spectra of ferric Cyt *c* in the region between 250 and 700 nm. In the presence of 5–20% PEG, almost no shift in the Soret peak at 409 nm was observed, suggesting that a dramatic conformational change around the heme center did not occur. We next confirmed whether Met80, a heme ligand, dissociated from the heme by observing the

ACCEPTED MANUSCRIPT

absorbance at 695 nm, which was derived from the S(Met80) → Fe charge-transfer transition. As shown in Figure 2B, the peak at 695 nm was not significantly affected by the concentration of PEG up to 20%, indicating that Met80 did not dissociate from the heme. These results clearly indicated that PEG did not partially denature Cyt *c*.

We characterized the structure of Cyt *c* in the presence of PEG using a variety of spectroscopic techniques. As shown in Figure 2C, the CD spectra in the far-UV region were insensitive to the PEG concentration, indicating that the secondary structure of Cyt *c* was not altered by the addition of PEG. In the absence of PEG, we observed a slightly asymmetric, negatively biased couplet with a minimum at 417 nm and a maximum at 406 nm in the Soret region of the CD spectrum (Figure 2D), in agreement with results obtained from horse heart Cyt *c* [28]. These signals did not change significantly with the PEG concentration up to 20%, consistent with the results observed in the absorption spectra (Figure 2A). We further measured the resonance Raman spectra of Cyt *c*. In the low-frequency region, some heme peripheral modes such as methyl, propionates, and thioether bonds, are observed [29]. Because some amino acid residues in Cyt *c* interact with the heme peripheral groups, we examined whether the PEG induced a structural change that alters such interactions. Figure 2E and 2F show the resonance Raman spectra of oxidized and reduced Cyt *c* in the absence and presence of PEG, respectively. The sharp bands at 396 and 691 $cm^{-1}$ in the oxidized state and 391 and 689 $cm^{-1}$ in the reduced state corresponded to the vibrations of the thioether linkages [$\delta(C_\beta C_a S)$] and C-S stretching $\nu(C_a S)$, respectively [29]. The intensity and frequency of these bands in a 20% PEG solution were very similar to those observed in the absence of PEG (Figure 2E and 2F). The spectroscopic data shown in Figures 2C, 2D, and 2E suggested that the geometry around the heme did not undergo a dramatic change upon the addition of PEG.

Next, we investigated whether tertiary structural changes, causing rapid autoxidation, occurred in Cyt *c* using fluorescence resonance energy transfer (FRET) measurements. The

ACCEPTED MANUSCRIPT

FRET efficiency ($E$) is determined by the fluorescence intensity transferred from a donor molecule to an acceptor molecule, and can be described as:

$$E = \frac{1}{1 + \left(r / R_0\right)^6} \tag{3}$$

where $R_0$ and $r$ are the fluorophore pair Förster distance and donor-to-acceptor separation distance, respectively. Assuming that the orientations of the dipole moments of the donor and heme are not altered during a conformational change, the fluorescence intensity from the donor would depend only on the distance between the donor and the heme according to an inverse 6$^{th}$ power law. Cyt *c* includes one tryptophan at position 59. Fluorescence from Trp59 is almost completely quenched by heme because it is located about 8 Å from the heme. Considering that the Förster distance between tryptophan and the heme is 29 Å [30], the FRET efficiency from Trp59 to heme is estimated to be nearly 100% (Equation 3). Thus, we introduced tryptophan at a position close to the $R_0$ value to improve the sensitivity of FRET to the distance between the heme and the tryptophan. Because Asp2 is located about 20 Å from the heme (Figure S1), we mutated Asp2 to Trp (D2W). Prior to measuring the fluorescence spectra, the $^{1}$H-$^{15}$N HSQC spectrum of the D2W mutant was measured to confirm whether the heme structural environment in the D2W mutant remained intact. As shown in Figure S2, except around the mutated position, the HSQC spectrum of the D2W mutant including heme periphery was essentially superimposable with that of the WT, indicating that this mutant possessed the similar tertiary structure and the same heme environmental structure as WT Cyt *c*.

The fluorescence spectra of the oxidized D2W mutant Cyt *c* in the presence of PEG are shown in Figure 3. The fluorescence signal at 350 nm was mainly derived from Trp2 because fluorescence from Trp59 was quenched by heme, as described above. As shown in Figure 3, the fluorescence intensity at 350 nm decreased significantly, by 23%, as the PEG concentration increased to 20%. Based on equation 3, a decrease in the fluorescence intensity

ACCEPTED MANUSCRIPT

was interpreted as a shortening of the distance between Trp2 and heme by 1.0 Å. The fluorescence spectra of the reduced D2W mutant in the presence of PEG were also measured (Figure S3) and showed the similar result: the fluorescence intensity at 350 nm decreased with increasing concentrations of PEG. We assumed that the environment around Trp2 was not affected by the addition of PEG because the fluorescence maximum of the D2W mutant was not shifted. Thus, our data suggested that PEG induced a conformational change that altered the relative positions of heme and Trp2 in Cyt *c*. Displacement of the heme appeared to occur.

We investigated whether conformational changes in Cyt *c* could be induced by the addition of other crowding agents. We selected trehalose as a second test crowder because it affects hydration in a manner that is distinct from that of PEG [31,32]. The fluorescence spectra of the D2W mutant in the presence of trehalose showed that the fluorescence intensity at 350 nm did not change significantly (Figure S4), indicating that the conformational changes accompanied by the change in the distance between Trp2 and heme did not occur in the presence of trehalose.

We further observed the oxidation reaction of Cyt *c* in a solution containing 5–20% trehalose by monitoring the absorbance at 550 nm. In contrast with the PEG solution, the absorbance at 550 nm did not change (Figure S5), indicating that trehalose did not promote oxidation of the Cyt *c* heme. Thus, the conformational changes associated with the displacement of the heme were induced only by the addition of PEG.

### 3.3. *Observation of dehydration induced by PEG*

Recent studies have proposed that high concentrations of several macromolecules or cosolutes should reduce the dielectric constant of an aqueous solvent, thereby inducing dehydration and conformational changes in proteins [15,16]. It is known that addition of 40% PEG causes the decrease in the relative dielectric constant of aqueous solution from 80 to 56

ACCEPTED MANUSCRIPT

[33], whereas 40% trehalose causes the decrease to 70 [34], indicating that the effect of on the relative dielectric constant was larger when PEG was added. Because heme is a strongly hydrophobic molecule, it prefers more hydrophobic environment. Therefore, the slight decrease in the dielectric constant can be one of the key factors for heme-displacement of Cyt *c*.

Based on these studies and the fact that PEG promotes dehydration at a protein surface [22–24], it is possible that PEG induced conformational changes in Cyt *c* by perturbing the hydration environment around the protein. We examined PEG-induced dehydration from Cyt *c* using near-infrared (NIR) spectroscopy. Figure 4A shows the NIR spectra of 50 μM Cyt *c* in a 50 mM sodium phosphate buffer. The broad band at 1450 nm corresponded to a combination of symmetric and asymmetric stretching vibrations in the water molecules[37]. The structural properties of the water molecules that hydrated Cyt *c* were investigated by subtracting the NIR spectrum of the buffer from that of Cyt *c* (Figure 4B). The difference spectrum revealed a positive peak at 1412 nm and a negative peak at 1490 nm, which were assigned to vibrations from the weakly and strongly hydrogen-bonded water, respectively [35,36]. The peaks at 1412 and 1490 nm in the difference spectrum between 10 μM Cyt *c* and the buffer were smaller than those in the difference spectrum between 50 μM Cyt *c* and the buffer. The peaks at 1412 and 1490 nm were postulated to be derived from water molecules that hydrated Cyt *c*. The difference spectra shown in Figure 4B reflect a structural change in the water molecules surrounding Cyt *c*: an increase in the number of the weakly hydrogen-bonded water molecules and a decrease in the number of the strongly hydrogen-bonded water molecules, upon the addition of Cyt *c*.

We next investigated the effect of PEG on the hydration state of Cyt *c*. We measured the NIR spectra of the buffer and 50 μM Cyt *c* in the presence of 5% PEG. Figure 4C shows the difference spectra obtained by subtracting the spectrum of the buffer from that of Cyt *c* in a PEG solution. The positive peak at 1412 nm decreased significantly in the presence of 5%

ACCEPTED MANUSCRIPT

PEG. This difference spectrum was similar to the difference spectrum obtained by subtracting the buffer spectrum from the Cyt *c* spectrum obtained in a 10% PEG solution. These results suggested that most of the water molecules that were weakly hydrogen-bonded to Cyt *c* were detached from the surface by PEG.

*3.4. Identification of the dehydration sites that caused heme displacement*

The dehydration sites on Cyt *c* were identified by focusing on the amino acid residues on the surface of Cyt *c*. As shown in Figure S6, most residues on the surface were hydrophilic, including lysine and arginine, and only a few hydrophobic residues were present near the heme. Our previous studies suggested that Ile81 and Val83 significantly contributed to the stabilization of the Cyt *c*-C*c*O complex by forming hydrophobic interactions upon dehydration [11,12]. We investigated whether the hydrophobic residues near the heme formed the primary dehydration region by performing site-directed mutagenesis experiments. Ile81 and Val83 was replaced with serine to alter the nature of hydration around position 81. Prior to verifying the hypothesis, the $^{1}H$-$^{15}N$ HSQC spectrum of the I81S mutant was measured to investigate the influence of the mutation on its tertiary structure. As shown in Figure S7, the chemical shift changes from several residues around the mutation site including near the heme periphery were observed. However, the resonance from Arg38, which is known to form a hydrogen bond with the propionate group of heme [37], did not shift, indicating that the tertiary structure of the I81S mutant was quite similar to that of WT.

We first measured the NIR spectra of the I81S mutant in the absence of PEG. The difference spectrum, obtained by subtracting the spectrum of the buffer from that of the I81S mutant, did not display a positive peak at 1412 nm (Figure 5A), unlike the WT Cyt *c* in the absence of PEG (Figure 4B). The difference spectrum of the I81S mutant, however, did resemble that of the WT in the presence of PEG (Figure 4C). A decrease in the positive peak

ACCEPTED MANUSCRIPT

at 1412 nm indicated that the replacement of hydrophobic isoleucine with hydrophilic serine reduced the number of weakly hydrogen-bonded water molecules around the mutation site in the absence of PEG. Considering that the NIR difference spectra of the WT Cyt *c* showed a decrease in the 1412 nm peak in the presence of PEG, the hydrophobic residue located near the heme periphery, Ile81, appeared to be a key dehydration sites.

We next investigated whether dehydration around the heme correlated with a change in the heme position (Figure 3) by replacing Asp2 of the I81S mutant with Trp and measuring the FRET efficiency in the presence of PEG. The I81S/D2W mutant was not well expressed in *E. coli*. Considering that Val83 was also located near the heme (Figure S6), we constructed a V83S/D2W double mutant. The $^{1}H$-$^{15}N$ HSQC spectrum of this mutant was also superimposable with that of WT Cyt *c* except the region around mutation site, meaning that the tertiary structure of the V83S/D2W mutant was also similar to that of WT. Figure 5B shows the fluorescence spectra of the V83S/D2W mutant in the presence of PEG. The fluorescence maximum at 350 nm, derived from Trp2, did not change significantly with the addition of PEG up to 20%, in contrast with the D2W mutant Cyt *c* (Figure 3). This result clearly indicated that the mutation of Val83 to serine suppressed the heme displacement. We also measured the NIR spectrum of the V83S mutant, showing that the difference spectrum, which was obtained by subtracting the spectrum of the buffer from that of the V83S mutant, was indistinguishable from that of the I81S mutant: a positive peak at 1412 nm was not observed (Figure 5A). These results suggest that the WT Cyt *c* heme position change in the presence of PEG was induced by dehydration around certain hydrophobic residues, including Ile81 and Val83.

The contributions of the heme displacement to the rapid autoxidation of heme were assessed by observing the oxidation of the I81S and V83S mutants in the 20% PEG solution. Figure 6C plots a comparison of the absorbance change at 550 nm for these mutants relative to that obtained from the WT after the addition of PEG. The observed oxidation rates of these

ACCEPTED MANUSCRIPT

mutants decreased significantly compared to that of the WT (Figure 5C). The NIR spectra of the I81S mutant (Figure 5A) and FRET measurements of the V83S/D2W mutant (Figure 5B) proposed that the reduced oxidation rates of these mutants resulted from suppressed heme displacement upon introduction of a hydrophilic serine moiety at the protein surface.

*3.5. Conformational changes in Cyt c associated with a change in the heme position*

We measured the two-dimensional $^{1}H$-$^{15}N$ HSQC spectra of $^{15}N$-labeled Cyt *c* in the absence or presence of 20% PEG to evaluate the changes in Cyt *c* induced by PEG. Figure 6A plots a superposition of the $^{1}H$-$^{15}N$ HSQC spectra of the oxidized Cyt *c* in the presence or absence of PEG. The addition of PEG increased the rotational correlation time by increasing the viscosity, resulting in overall line broadening. A specific decrease in the peak intensity was also observed in the resonances from Cys14, Cys17, His18, Thr19, Val20, Gly29, Glu61, Gly77, Thr78, Lys79, Met80, Ile81, and Phe82, most of which were located near the heme.

In addition to the specific line broadening, some peaks displayed chemical shift perturbations upon the addition of PEG, reflecting environmental changes. Figure 6B plots the chemical shift perturbations measured at the backbone amides of Cyt *c* upon the addition of PEG. The N-H cross-peaks from Met12, Gln16, Cys17, His18, Arg38, Gly56, Glu61, Gly77, Phe82, Val83, and Lys86 were substantially shifted. These chemical shift changes were interpreted as local tertiary conformational changes and/or direct contact with PEG. In fact, several reports have proposed that longer chain PEG (e.g. PEG 5,000) can nonspecifically interact with hydrophobic proteins due to the presence of a hydrophobic methylene group in PEG [38–40]. In our study, however, the residues perturbed by the presence of PEG included several surface-exposed hydrophilic residues (Gln16, Glu61, and Lys86) as well as hydrophobic residues, suggesting that PEG did not specifically perturb the hydrophobic residues. Moreover, the residues exhibiting the chemical shift perturbations upon the addition

ACCEPTED MANUSCRIPT

of PEG were mainly gathered in the heme periphery region (Figure 6C). These chemical shift changes were, therefore, interpreted as resulting from local perturbations in the surface-exposed residues rather than from nonspecific direct contact with PEG.

As described above, the distributions of chemical shift perturbations induced by PEG were mapped onto the structure of Cyt *c*, as shown in Figure 6C. Most of the perturbed residues were located near the exposed hydrophobic heme edge, in agreement with results reported from *Saccharomyces cerevisiae* Cyt *c* [41]. Considering that PEG induced changes in the heme position (Figure 3), the chemical shift perturbations near the heme of Cyt *c* observed upon the addition of 20% PEG (Figure 6B and 6C) were attributed to tertiary structural changes that accompanied the heme displacement. By contrast, none of the peaks showed chemical shift perturbations upon the addition of 20% trehalose (Figure S9). These results indicated that the residues located near the heme were not affected by trehalose. Therefore, the heme-displacement of Cyt *c* shown in Figure 6B and 6C was induced by only addition of PEG, which facilitates dehydration from the surface of Cyt *c*.

The $^{1}H$-$^{15}N$ HSQC spectra of the I81S mutant were measured in the absence and presence of PEG. The residues that displayed chemical shift perturbations upon the addition of PEG are displayed in Figures 6D and 6E. The PEG-induced chemical shift perturbations observed in the I81S mutant were similar to those observed in the WT Cyt *c* (Figure 6B or 6C). These observations were somewhat unexpected because our FRET measurements indicated that the heme position of the V83S/D2W mutant Cyt *c* did not change in the PEG solution (Figure 5B). These results of the HSQC spectra in the I81S mutant implied that the perturbation of heme also occurred in the I81S mutant. In this mutant, however, the chemical shift changes observed in Gly77, Val83, and Lys86, which are located near heme, decreased substantially compared to the changes observed in WT Cyt *c*. The spectroscopic data obtained from the I81S mutant suggested that the PEG-induced changes in the local protein conformation around the mutation site were specifically suppressed by the presence of serine. Suppression

ACCEPTED MANUSCRIPT

of the tertiary conformational changes in the I81S mutant reflected the independence of the autoxidation rate from the PEG concentration.

We measured the $^{1}$H NMR spectra of Cyt *c* in the presence of PEG to investigate the PEG-induced environmental changes around the heme in Cyt *c*. As shown in Figure S10, the signals from the porphyrin ring (3-methyl, 8-methyl, and 7-propionate) and axial ligands (His18 and Met80) shifted as the PEG concentration increased. The signal from the 3-methyl group on the heme, in particular, displayed a more prominent shift than was observed from 8-methyl or 7-propionate. Considering that the surface-exposed hydrophobic residues (Ile81 and Val83) were located near the 3-methyl (Figure S6), these data support the suggestion that the addition of PEG induced tertiary conformational changes around Ile81 and Val83 near the 3-methyl group of heme.

*3.6. Influence of heme-displacement on its redox potential*

Finally, we conducted spectroelectrochemical redox titration of Cyt *c* in the absence and presence of PEG to investigate the effect of the PEG-induced tertiary structural change of Cyt *c* on the rapid oxidation. The plots of the relative ratio of the reduced heme against the measured potential in the absence or presence of PEG are shown in Figure 7A and 7B, respectively. For the titration, the fit of the relative ratio of the reduced heme to the Nernst equation yielded midpoint reduction potential, $E_m$. As shown in Figure 7A and 7B, the reductive and oxidative titration curves were superimposed, which indicates that the redox process was reversible. In the absence of PEG, the $E_m$ potential of Cyt *c* was estimated to be +236 ± 3 mV vs NHE (Figure 7A), in agreement with the results obtained from horse heart Cyt *c* of +235 mV [42]. On the other hand, the $E_m$ potential of human Cyt *c* in the presence of 20% PEG was found to be +200 ± 4 mV vs NHE (Figure 7B). This corresponded to a downshift by approximately 40 mV of Cyt *c* upon the addition of PEG.

ACCEPTED MANUSCRIPT

## 4. Discussion

### *4.1. Explanation for the rapid autoxidation of heme iron in the presence of PEG*

In this paper, we found that the heme iron of Cyt *c* was rapidly oxidized in the presence of 5–20% PEG (Figure 1). The oxidation rate of reduced Cyt *c* was recently reported to increase through interactions with the mitochondrial lipid, cardiolipin (CL) [43,44]. The absorption spectra of reduced Cyt *c* in the presence of 200 μM CL exhibited a blue shift in the Soret maximum, from 413.5 to 408.5 nm, which suggested that CL induced a conversion to a non-native state [44–46]. In this case, the absorbance at 695 nm decreased as the CL concentration increased. Additionally, the CD signal was altered from a couplet to a positive Cotton effect band, reflecting a transition from a native state to a partially unfolded state [44,46,47]. Especially, Bradley reported that in the reduced Cyt *c*-CL complex, the major conformer (80%) contains high-spin heme iron, suggesting that heme is predominantly five-coordinate, but not six-coordinate, in the presence of CL and thus readily binds small exogenous ligands such as $O_2$ [48]. Basova et al. measured the redox potential of Cyt *c* in the presence of CL using cyclic voltammetry and showed a negative shift in the redox potential by 350–400 mV upon binding to CL-containing membranes. They further found that the reduction rate of Cyt *c* in the presence of CL was 60-fold smaller than that in the absence of CL [49]. These extensive measurements indicated that the interactions between Cyt *c* and CL induced partial denaturation around the heme and were associated with the disruption of the Fe-Met80 linkage, resulting in a negative shift in the redox potential and a decrease in the reduction rate of Cyt *c*.

In the presence of PEG, neither the absorption nor CD spectra of Cyt *c* changed (Figure 2A, 2B, and 2D). The resonance Raman spectra of both oxidized and reduced Cyt *c* in the presence of PEG were almost identical to those in the absence of PEG (Figure 2E and 2F).

ACCEPTED MANUSCRIPT

The addition of PEG at concentrations up to 20% did not induce significant perturbations in the backbone resonances of Cyt *c*, supporting the notion that the overall structure of Cyt *c* was preserved in the presence of PEG (Figure 6A). The acceleration of Cyt *c* autoxidation in the presence of PEG was not, therefore, derived from partial denaturation (dissociation of Met80 from heme), as is observed in the presence of CL. The PEG-induced acceleration of Cyt *c* autoxidation disappeared under anaerobic conditions, indicating that molecular oxygen is an electron acceptor. Because Cyt *c* has a six-coordinate heme center (His/Met), it does not readily form $O_2$-bound heme, as is observed in myoglobin and hemoglobin. In the presence of PEG or sugar, such as fructose and glucose, the solubility of $O_2$ is decreased [50,51], which should lead to slower autoxidation. However, PEG induced a significant increase in the autoxidation rate (Figure 1). Previous studies of cytochrome $b_5$ (Cyt $b_5$) autoxidation showed that Cyt $b_5$ is rapidly oxidized under aerobic conditions without partial denaturation, despite including six-coordinate bis-His ligation [52]. They suggested that the iron-$O_2$ bond is neither a prerequisite nor an intermediate for Cyt $b_5$ autoxidation. In our study, the mechanism by which Cyt *c* was autoxidized in the presence of PEG is analogous to that of Cyt $b_5$, in which electron transfer occurs via an outer sphere pathway.

On the other hand, the decreased absorbance at 550 nm for the I81S and V83S mutants upon the addition of PEG was significantly suppressed compared to that observed for the WT Cyt *c* (Figure 5C), indicating that the observed Cyt *c* oxidation rate decreased upon mutation of the surface-exposed residues (Ile81 or Val83) near the heme with serine. Furthermore, the NIR difference spectra obtained by subtracting the spectrum of the buffer from that of the I81S and V83S mutants in the absence or presence of PEG did not exhibit a positive peak at 1412 nm, observed in WT Cyt *c* with a decreased intensity upon the addition of PEG (Figures 4C and 5A). These results suggested that hydrated water molecules around the mutation site at position 81 were not dehydrated, even in the presence of PEG, unlike the results observed for WT. Altogether, dehydration from Ile81 and Val83 is likely to be a key contributor to the

ACCEPTED MANUSCRIPT

increased Cyt *c* oxidation rate.

*4.2. Conformational changes in Cyt c induced by dehydration*

The effects of dehydration from the surface-exposed hydrophobic residues (Ile81 and Val83) on autoxidation were investigated by examining the tertiary structural changes observed in Cyt *c* in the presence of PEG. As shown in Figure 3, the fluorescence intensity at 350 nm from Trp2 was gradually quenched by heme as the PEG concentration increased, indicating a shortening of the distance between Trp2 and heme. Considering that Trp2 was exposed to solvent, and the fluorescence maximum of Trp2 was not shifted by the addition of PEG, a decrease in the fluorescence intensity at 350 nm appeared to originate from tertiary conformational changes accompanied by displacement of the heme. High concentrations of PEG are known to induce a decrease in the dielectric constant in an aqueous solvent, causing dehydration from the surfaces of proteins [16,22]. A recent study of the structures of several polypeptides in a cellular environment suggested that a decrease in the dielectric constant alters the polypeptide conformation and exposes its hydrophobic components to solvent [15]. A notable structural characteristic of Cyt *c* is that the hydrophobic 3-methyl group of the *c*-type heme is fully exposed to solvent (Figure S6). Hydrophobic surface residues, such as Ile81 and Val83, are proximal to the 3-methyl group of heme, and mutation of these residues to serine was found to suppress heme displacement (Figure 5B).

The NMR spectra of WT Cyt *c* in the presence of PEG revealed that the N-H cross peaks from the residues near the 3-methyl group of heme, Met12, Gln16, Cys17, Phe82, and Val83, were substantially shifted upon the addition of PEG (Figure 6B and 6C), and mutation of Ile81 to serine reduced the chemical shift perturbations of Phe82 and Val83 (Figures 6D and 6E). The signal from the 3-methyl group of heme exhibited a substantial shift upon the addition of PEG (Figure S10). These results suggested that the addition of PEG dehydrated

ACCEPTED MANUSCRIPT

the hydrophobic surface residues near the 3-methyl group of heme, Ile81 and Val83, leading to a change in the heme position (Figure 8A).

The NIR difference spectrum obtained by subtracting the spectrum of the buffer from that of the Cyt *c* solution in the presence of trehalose (Figure S11) was similar to that obtained from the I81S and V83S mutant: the positive peak at 1412 nm was not observed. These results indicated that the structure of the hydration water molecules did not change by the addition of Cyt *c* in the presence of trehalose. Furthermore, as shown in Figure S4 and S9, the conformational changes accompanied by the heme displacement were not observed in the presence of trehalose. The $^{1}$H NMR spectra obtained from the porphyrin ring and axial ligands of Cyt *c* in the presence of trehalose (Figure S12) did not display significant chemical shifts compared with those observed in the presence of PEG (Figure S10). These results indicated that the heme displacement was induced by only adding PEG, which promotes dehydration from the surface of Cyt *c*.

*4.3. Functional significance of dehydration to electron transfer*

Finally, we deduced the contribution of the heme displacement induced by dehydration from Ile81 and Val83 to the increase in the oxidation rate of Cyt *c*. The oxidation/reduction rates of Cyt *c* are known to be dominated by its redox potential [49] and/or small changes in the tertiary structure [53]. Gray and co-workers analyzed the redox potentials of eight structurally characterized *c*-type cytochromes and proposed that the redox potentials of Cyt *c* could be tuned by roughly 500 mV by varying the heme exposure to solvent [54]. Fantuzzi et al. investigated the relationship between the reduction potential and the accessible surface area (ASA) of the Cyt $c_{553}$ heme [55]. They mutated Met23 or Gly51, which are located near heme and exposed to solvent, to Cys residues and constructed M23C-M23C or G51C-G51C homodimers through specific disulfide bridge formation to decrease the ASA of heme.

ACCEPTED MANUSCRIPT

Potentiometric titration of the Cyt $c_{553}$ mutants showed that the reduction potential shifted toward positive values, from 20 to 105 mV, as the ASA decreased from 73 to 50 Å$^2$. These results indicated that the less solvent-exposed heme was more stable in the reduced state. In the case of human Cyt *c*, the redox titration showed the decrease in the $E_m$ by approximately 40 mV by the addition of PEG (Figure 7). Considering the slight shift in the heme position by approximately 1.0 Å (Figure 3), PEG would induce a slight change of heme position to a solvent-exposed region, thereby moderately increasing the ASA of heme and decreasing the reduction potential of the Cyt *c*, although the detailed correlation between the redox potential and ASA remains to be elucidated. The observed negative shift in the redox potential of heme was expected to accelerate its oxidation.

As described above, heme displacement of Cyt *c* in the presence of PEG was thought to be induced by dehydration of the surface-exposed hydrophobic residues, Ile81 and Val83. On the other hand, previous mechanistic studies of the formation of the Cyt *c*-C*c*O complex proposed that hydrated water molecules around Ile81 and Val83 were expelled when Cyt *c* forms a complex with C*c*O through hydrophobic interactions [12]. The tertiary structural changes that accompanied the heme displacement upon the addition of PEG were estimated based on the $^1$H-$^{15}$N HSQC spectra (Figures 6B and 6C). Chemical shift changes or line broadening upon the addition of PEG were observed on Met12, Gln16, Cys17, His18, Lys79, Met80, Ile81, Phe82, Val83, and Lys86. A previous NMR spectroscopy study revealed the interaction sites between Cyt *c* and C*c*O[11]. The chemical shift changes or line broadening observed upon the addition of C*c*O were observed at the residues located near the heme, Met12, Cys17, His18, Lys79, Met80, Ile81, Val83, and Lys86, as well as several positively or negatively charged residues. These results suggested that the tertiary conformational changes at the heme periphery in the presence of PEG were similar to those involved in Cyt *c*-C*c*O complex formation. These tertiary conformational changes would provide evidence for heme displacement of Cyt *c* during Cyt *c*-C*c*O complexation. We propose the following hypothesis:

ACCEPTED MANUSCRIPT

PEG-induced dehydration from the surface of Cyt *c* partially mimicked dehydration at the interaction sites of Cyt *c* with C*c*O (Figure 8B), and when Cyt *c* associated with C*c*O, heme was displaced to solvent upon dehydration of Ile81 and Val83, leading to a negative shift in the heme redox potential by approximately 40 mV.

## 5. Conclusion

In summary, we unexpectedly found that the Cyt *c* heme was rapidly oxidized in the presence of PEG. The molecular mechanism underlying the Cyt *c* autoxidation was explored by characterizing the structure of Cyt *c* in the presence of PEG. UV-visible absorption, CD, and resonance Raman spectra of Cyt *c* indicated that the rapid autoxidation was not derived from partial denaturation. Fluorescence spectra of the D2W mutant revealed a tertiary conformational change, including heme displacement, which was further supported by the NMR spectra collected in the presence of PEG. Our NIR spectra and various site-directed mutagenesis studies proposed that heme displacement in the presence of PEG was induced by dehydration from the surface-exposed hydrophobic residues (Ile81 and Val83) located near heme. Considering previous results, which indicated that these hydrophobic residues were the primary sites dehydrated upon formation of the complex between Cyt *c* and C*c*O, tertiary conformational changes in Cyt *c* with heme displacement were expected to occur upon Cyt *c*-C*c*O complexation, which negatively shifted the reduction potential by increasing the ASA of heme. Considering the small differences in the redox potential between the electron donor (Cyt *c*, +235 mV) and acceptor ($Cu_A$ of C*c*O, +245 mV) [42] and the long distance between the thioether group of heme *c* in Cyt *c* and the aromatic carbon atom of Trp104 in subunit II of C*c*O (15.6 Å) [12], this negative shift in the reduction potential of Cyt *c* by approximately 40 mV observed in the presence of 20% PEG is expected to contribute to efficient electron donation to C*c*O. The findings of this work suggest the importance of the hydration water

ACCEPTED MANUSCRIPT

structure on the structures and functions of proteins under physiological conditions.

**Associated content**

**Ⓢ Supporting Information**

The Supporting Information is available free of charge on the ACS Publications website at DOI:

Additional data including UV-visible absorption and NMR spectra, view of Cyt *c* characteristics, order parameters, and further information (PDF)

**Author information**

**Corresponding Authors**

*Takeshi Uchida

Department of Chemistry, Faculty of Science, Hokkaido University, Sapporo 060-0810, Japan. Phone: +81-11-706-3501, E-mail: uchida@sci.hokudai.ac.jp,

*Koichiro Ishimori

Department of Chemistry, Faculty of Science, Hokkaido University, Sapporo 060-0810, Japan. Phone: +81-11-706-2707, E-mail: koichiro@sci.hokudai.ac.jp

**Funding**

This study was supported in part by Grants-in-Aid for Scientific Research (16H04173 to K.I. and 15K20829 to T.S.) from the Ministry of Culture, Education, Sports, Science, and Technology (MEXT) of Japan.

**Notes**

The authors declare no competing financial interest.

**Acknowledgments**

We would like to thank Dr. Hiroyuki Kumeta for the help in NMR experiment. Some of NMR experiments were performed at the Advanced NMR Facility, Hokkaido University.

**Abbreviation**

Cyt *c*, cytochrome *c*; C*c*O, cytochrome *c* oxidase; PEG, polyethylene glycol; FRET,

ACCEPTED MANUSCRIPT

fluorescence resonance energy transfer; WT, wild-type; NIR, near-infrared; Cyt $b_5$, cytochrome $b_5$.

**References**


[1] S. Yoshikawa, A. Shimada, Reaction mechanism of cytochrome *c* oxidase, Chem. Rev., 115 (2015) 1936–1989.

[2] F. Malatesta, G. Antonini, P. Sarti, M. Brunori, Structure and function of a molecular machine: cytochrome *c* oxidase, Biophys. Chem., 54 (1995) 1–33.

[3] S. Papa, Molecular mechanism of proton translocation by the cytochrome system and the ATPase of mitochondria. Role of proteins, J. Bioenerg. Biomembr., 14 (1982) 69–86.

[4] S. Ferguson-Miller, D.L. Brautigan, E. Margoliash, Definition of cytochrome binding domains by chemical modification. III Kinetics of reaction of carboxydinitrophenyl cytochromes *c* with cytochrome *c* oxidase, J. Biol. Chem., 253 (1978) 149–159.

[5] P. Lappalainen, N.J. Watmough, C. Greenwood, M. Saraste, Electron transfer between cytochrome *c* and the isolated $Cu_A$ domain: Identification of substrate-binding residues in cytochrome *c* oxidase, Biochemistry, 34 (1995) 5824–5830.

[6] H. Witt, F. Malatesta, F. Nicoletti, M. Brunori, B. Ludwig, Cytochrome-*c*-binding site on cytochrome oxidase in *Paracoccus denitrificans*, Eur. J. Biochem., 251 (1998) 367–373.

[7] V. Drosou, F. Malatesta, B. Ludwig, Mutations in the docking site for cytochrome *c* on the *Paracoccus* heme $aa_3$ oxidase: Electron entry and kinetic phases of the reaction, Eur. J. Biochem., 269 (2002) 2980–2988.

[8] S. Döpner, P. Hildebrandt, F.I. Rosell, A.G. Mauk, M. von Walter, G. Buse, T. Soulimane, The structural and functional role of lysine residues in the binding domain of cytochrome *c* in the electron transfer to cytochrome *c* oxidase, Eur. J. Biochem., 261 (1999) 379–391.

[9] K. Wang, Y. Zhen, R. Sadoski, S. Grinnell, L. Geren, S. Ferguson-Miller, B. Durham, F. Millett, Definition of the interaction domain for cytochrome *c* on cytochrome *c* oxidase II Rapid kinetic analysis of electron transfer from cytochrome c to Rhodobacter sphaeroides cytochrome oxidase surface mutants, J. Biol. Chem., 274 (1999) 38042–38050.

[10] J.T. Hazzard, S. Rong, G. Tollin, Ionic strength dependence of the kinetics of electron transfer from bovine mitochondrial cytochrome *c* to bovine cytochrome *c* oxidase, Biochemistry, 30 (1991) 213–222.

[11] K. Sakamoto, M. Kamiya, M. Imai, K. Shinzawa-Itoh, T. Uchida, K. Kawano, S. Yoshikawa, K. Ishimori, NMR basis for interprotein electron transfer gating between cytochrome *c* and cytochrome *c* oxidase, Proc. Natl. Acad. Sci. U. S. A., 108 (2011)

ACCEPTED MANUSCRIPT

12271–12276.

[12] W. Sato, S. Hitaoka, K. Inoue, M. Imai, T. Saio, T. Uchida, K. Shinzawa-Itoh, S. Yoshikawa, K. Yoshizawa, K. Ishimori, Energetic mechanism of cytochrome *c*-cytochrome *c* oxidase electron transfer complex formation under turnover conditions revealed by mutational effects and docking simulation, J. Biol. Chem., 291 (2016) 15320–15331.

[13] I. Jelesarov, H.R. Bosshard, Thermodynamics of ferredoxin binding to ferredoxin:$NADP^+$ reductase and the role of water at the complex interface, Biochemistry, 33 (1994) 13321–13328.

[14] R.J. Ellis, A.P. Minton, Join the crowd, Nature, 425 (2003) 27–28.

[15] S. Tanizaki, J. Clifford, B.D. Connelly, M. Feig, Conformational sampling of peptides in cellular environments, Biophys. J., 94 (2008) 747–759.

[16] R. Harada, Y. Sugita, M. Feig, Protein crowding affects hydrations structure and dynamics, J. Am. Chem. Soc., 134 (2012) 4842–4849.

[17] H. Zhou, G. Revas, A.P. Minton, Macromolecular crowding and confinement : Biochemical , biophysical , and potential physiological consequences, Annu. Rev. Biophys., 37 (2008) 375–397.

[18] N. Kozer, G. Schreiber, Effect of crowding on protein-protein association rates: fundamental differences between low and high mass crowding agents, J. Mol. Biol., 336 (2004) 763–774.

[19] T. Díaz-López, C. Dávila-Fajardo, F. Blaesing, M.P. Lillo, R. Giraldo, Early events in the binding of the pPS10 replication protein RepA to single iteron and operator DNA sequences, J. Mol. Biol., 364 (2006) 909–920.

[20] L.A. Munishkina, E.M. Cooper, V.N. Uversky, A.L. Fink, The effect of macromolecular crowding on protein aggregation and amyloid fibril formation, J. Mol. Recognit., 17 (2004) 456–464.

[21] B. van den Berg, R. Wain, C.M. Dobson, R.J. Ellis, Macromolecular crowding perturbs protein refolding kinetics: implications for folding inside the cell, EMBO J., 19 (2000) 3870–3875.

[22] P.K. Verma, S. Rakshit, R.K. Mitra, S.K. Pal, Role of hydration on the functionality of a proteolytic enzyme α-chymotrypsin under crowded environment, Biochimie, 93 (2011) 1424–1433.

[23] J.R. Giorgione, R.M. Epand, Role of water in protein kinase C catalysis and its binding to membranes, Biochemistry, 36 (1997) 2250–2256.

[24] R.P. Rand, N.L. Fuller, P. Butko, G. Francis, P. Nicholls, Measured change in protein solvation with substrate binding and turnover, Biochemistry, 32 (1993) 5925–5929.

[25] W.-Y. Jeng, C.-Y. Chen, H.-C. Chang, W.-J. Chuang, Expression and characterization of recombinant human cytochrome *c* in *E coli*, J. Bioenerg. Biomembr., 34 (2002) 423–431.

ACCEPTED MANUSCRIPT

[26] F. Delaglio, S. Grzesiek, G.W. Vuister, G. Zhu, J. Pfeifer, A. Bax, NMRPipe: A multidimensional spectral processing system based on UNIX pipes, J. Biomol. NMR, 6 (1995) 277–293.

[27] F.A. Mulder, D. Schipper, R. Bott, R. Boelens, Altered flexibility in the substrate-binding site of related native and engineered high-alkaline *Bacillus* subtilisins, J. Mol. Biol., 292 (1999) 111–123.

[28] I. Dragomir, A. Hagarman, C. Wallace, R. Schweitzer-Stenner, Optical band splitting and electronic perturbations of the heme chromophore in cytochrome *c* at room temperature probed by visible electronic circular dichroism spectroscopy, Biophys. J., 92 (2007) 989–998.

[29] S. Hu, I.K. Morris, J.P. Singh, K.M. Smith, T.G. Spiro, Complete assignment of cytochrome *c* resonance Raman spectra via enzymatic reconstitution with isotopically labeled hemes, J. Am. Chem. Soc., 115 (1993) 12446–12458.

[30] P.G. Wu, L. Brand, Resonance energy transfer: Methods and applications, Anal. Biochem., 218 (1994) 1–13.

[31] C. Olsson, H. Jansson, J. Swenson, The role of trehalose for the stabilization of proteins, J. Phys. Chem. B, 120 (2016) 4723–4731.

[32] M. Auton, D.W. Bolen, J. Rösgen, Structural thermodynamics of protein preferential solvation: Osmolyte solvation of proteins, aminoacids, and peptides, Proteins Struct. Funct. Genet., 73 (2008) 802–813.

[33] K. Arnold, A. Herrmann, L. Pratsch, K. Gawrisch, The dielectric properties of aqueous solutions of poly(ethylene glycol) and their influence on membrane structure, Biochim. Biophys. Acta, Biomembr., 815 (1985) 515–518.

[34] M.P. Longinotti, H.R. Corti, Fractional Walden rule for electrolytes in supercooled disaccharide aqueous solutions, J. Phys. Chem. B, 113 (2009) 5500–5507.

[35] V.H. Segtnan, T. Isaksson, Y. Ozaki, Studies on the structure of water using spectroscopy and principal component analysis, Anal. Chem., 73 (2001) 3153–3161.

[36] E. Chatani, Y. Tsuchisaka, Y. Masuda, R. Tsenkova, Water molecular system dynamics associated with amyloidogenic nucleation as revealed by real time near infrared spectroscopy and aquaphotomics, PLoS One, 9 (2014) 1–10.

[37] L. Muresanu, P. Pristovšek, F. Löhr, O. Maneg, M.D. Mukrasch, H. Rüterjans, B. Ludwig, C. Lücke, The electron transfer complex between cytochrome $c_{552}$ and the CuA domain of the *Thermus thermophilus* $ba_3$ oxidase: A combined NMR and computational approach, J. Biol. Chem., 281 (2006) 14503–14513.

[38] A. Hirano, K. Shiraki, T. Arakawa, Polyethylene glycol behaves like weak organic solvent, Biopolymers, 97 (2011) 117–122.

[39] J. Wu, C. Zhao, W. Lin, R. Hu, Q. Wang, H. Chen, L. Li, S. Chen, J. Zheng, Binding characteristics between polyethylene glycol (PEG) and proteins in aqueous solution, J. Mater. Chem. B, 2 (2014) 2983–2992.

ACCEPTED MANUSCRIPT

[40] A.J. Keefe, S. Jiang, Poly(zwitterionic)protein conjugates offer increased stability without sacrificing binding affinity or bioactivity, Nat. Chem., 4 (2011) 59–63.

[41] P.B. Crowley, K. Brett, J. Muldoon, NMR spectroscopy revceals cytochrome *c*-poly(ethylene glycol) interactions, ChemBioChem, 9 (2008) 685–688.

[42] D.F. Wilson, M. Erecinska, P.L. Dutton, Thermodynamic relationships in mitochondrial oxidative phosphorylation, Annu. Rev., (1974) 203–230.

[43] H. Iwase, T. Takatori, M. Nagao, K. Iwadate, M. Nakajima, Monoepoxide production from linoleic acid by cytochrome *c* in the presence of cardiolipin, Biochem Biophys Res Commun, 222 (1996) 83–89.

[44] L. Serpas, B. Milorey, L.A. Pandiscia, A.W. Addison, R. Schweitzer-Stenner, Autoxidation of reduced horse heart cytochrome *c* catalyzed by cardiolipin-containing membranes, J. Phys. Chem. B, 120 (2016) 12219–12231.

[45] S. Oellerich, H. Wackerbarth, P. Hildebrandt, Spectroscopic characterization of nonnative conformational states of cytochrome *c*, J. Phys. Chem. B, 106 (2002) 6566–6580.

[46] L.A. Pandiscia, R. Schweitzer-Stenner, Coexistence of native-like and non-native partially unfolded ferricytochrome *c* on the surface of cardiolipin-containing liposomes, J. Phys. Chem. B, 119 (2015) 1334–1349.

[47] A. Hagarman, L. Duitch, R. Schweitzer-Stenner, The conformational manifold of ferricytochrome *c* explored by visible and far-UV electronic circular dichroism spectroscopy, Biochemistry, 47 (2008) 9667–9677.

[48] J.M. Bradley, G. Silkstone, M.T. Wilson, M.R. Cheesman, J.N. Butt, Probing a complex of cytochrome *c* and cardiolipin by magnetic circular dichroism spectroscopy: Implications for the initial events in apoptosis, J. Am. Chem. Soc., 133 (2011) 19676–19679.

[49] L. V. Basova, I. V. Kurnikov, L. Wang, V.B. Ritov, N.A. Belikova, I.I. Vlasova, A.A. Pacheco, D.E. Winnica, J. Peterson, H. Bayir, D.H. Waldeck, V.E. Kagan, Cardiolipin switch in mitochondria: Shutting off the reduction of cytochrome *c* and turning on the peroxidase activity, Biochemistry, 46 (2007) 3423–3434.

[50] P. Ji, W. Feng, T. Tan, D. Zheng, Modeling of water activity, oxygen solubility and density of sugar and sugar alcohol solutions, Food Chem., 104 (2007) 551–558.

[51] J. Mexal, J.T. Fisher, J. Osteryoung, C.P. Reid, Oxygen availability in polyethylene glycol solutions and its implications in plant-water relations, Plant Physiol., 55 (1975) 20–24.

[52] M.C. Berman, C.M. Adnams, K.M. Ivanetich, J.E. Kench, Autoxidation of soluble trypsin-cleaved microsomal ferrocytochrome $b_5$ and formation of superoxide radicals, Biochem J, 157 (1976) 237–246.

[53] F. Wegerich, P. Turano, M. Allegrozzi, H. Möhwald, F. Lisdat, Cytochrome *c* mutants for superoxide biosensors, Anal. Chem., 81 (2009) 2976–2984.

ACCEPTED MANUSCRIPT

[54] F.A. Tezcan, J.R. Winkler, H.B. Gray, Effects of ligation and folding on reduction potentials of heme proteins, J. Am. Chem. Soc., 120 (1998) 13383–13388.

[55] A. Fantuzzi, S. Sadeghi, F. Valetti, G.L. Rossi, G. Gilardi, Tuning the reduction potential of engineered cytochrome *c*-553, Biochemistry, 41 (2002) 8718–8724.

ACCEPTED MANUSCRIPT

ACCEPTED MANUSCRIPT

**Conflict of interest:**

**The authors declare that they have no conflict of interest with the contents of this article.**

ACCEPTED MANUSCRIPT

ACCEPTED MANUSCRIPT

**Figure 1**. **Absorbance changes at 550 nm after addition of PEG 4000.** The measurements were performed by mixing of 3 μM ferrous Cyt *c* and 0 (black), 5 (red), 10 (yellow), 15 (green), and 20 (blue)% solutions of PEG, dissolved in 50 mM sodium phosphate buffer (pH 7.0) at 293 K under aerobic conditions.

**Figure 2. UV-visible absorption, CD, and resonance Raman spectra of Cyt *c* in the presence of PEG.** Absorption spectra in the region between 250 and 700 nm of 8 μM oxidized Cyt *c* (A) and between 600 and 800 nm of 0.3 mM oxidized Cyt *c* (B). CD spectra in the far-UV region of 2 μM Cyt *c* (C) and in the Soret region of 10 μM Cyt *c* (D). These measurements were carried out in the presence of 0% (black), 5% (red), 10% (yellow), 15% (green), and 20% (blue) PEG. (E) (F) Resonance Raman spectra in the low frequency region of 50 M oxidized (E) and reduced (F) Cyt *c*. These measurements were carried out in the presence of 0% (red) and 20% (blue) PEG. For all measurements, samples were dissolved in 50 mM sodium phosphate buffer (pH 7.0) at 293 K.

**Figure 3**. **Fluorescence spectra for the oxidized D2W mutant Cyt *c***. The measurements were carried out in the presence of 6 μM Cyt *c* with 0 (red), 10 (blue), and 20 (green)% solutions of PEG, dissolved in 50 mM sodium phosphate buffer (pH 7.0) at 293 K.

**Figure 4. NIR spectra of Cyt *c* in the region between 1300 and 1600 nm.** (A) NIR spectra in the absence (black) and presence of 50 mM Cyt *c* (red) dissolved in 50 mM sodium phosphate buffer (pH 7.0) at 293 K. (B) Difference NIR spectra subtracting the spectrum of buffer from that of 50 μM Cyt *c* (red) and that of 10 μM Cyt *c* (black). (C) Difference NIR spectra subtracting the spectra of buffer including 0 (red), 5 (blue), and 10% (green) PEG from that of 50 μM Cyt *c* in 0 (red), 5 (blue), and 10% (green) PEG solution.

**Figure 5. Difference NIR spectra, fluorescence spectra, and absorbance change at 550 nm of mutants Cyt *c* in the presence of PEG.** (A) Difference NIR spectra subtracting the spectra of buffer including 0 (red), 5 (blue), and 10% (green) PEG from that of 50 μM V83S in buffer (orange) and I81S mutant Cyt *c* in 0 (red), 5 (blue), and 10% (green) PEG solution. The experimental conditions were the same as Figure 4C. (B) Fluorescence spectra for D2W/V83S mutant Cyt *c* in the presence of 0 (red), 10 (blue), and 20% (green) PEG. The experimental conditions were the same as Figure 3. (C) Absorbance changes at 550 nm of WT (red), I81S (blue), and V83S (green) Cyt *c* after addition of 5% PEG. The experimental conditions were the same as Figure 1.

**Figure 6**. **Chemical shift perturbation in Cyt *c* in the presence of PEG.** (A) Superposition of the $^{1}$H-$^{15}$N HSQC spectra of $^{15}$N-labeled Cyt *c* in the absence (red) and presence of PEG (blue). Overview of the combined backbone chemical shift changes (bar graph) and line broadening (asterisk) of WT (B) and I81S mutant (D) Cyt *c* induced by addition of 20% PEG. Mapping of the affected residues on the surface of WT (C) and I81S mutant (E) Cyt *c*. The residues with chemical shift changes of $x \geq 0.042$, $0.042 > x \geq 0.037$, $0.037 > x \geq 0.032$, and $0.032 > x \geq 0.027$ are colored in orange, yellow, green, and cyan, respectively. In

ACCEPTED MANUSCRIPT

addition, red color represents the residues showing the specific line broadening. The measurements were carried out in the presence of 0.15 mM WT (B) or I81S (D) Cyt *c* with 0 and 20% solutions of PEG, dissolved in 50 mM sodium phosphate buffer (pH 7.0) at 293 K.

**Figure 7. Spectroelectrochemical redox titration of Cyt *c* in the (A) absence and (B) presence of 20% PEG.** The potential of electrode was decrease in 50 mV step from +500 to –100 mV vs NHE (red) and then increase from –100 to +500 mV vs NHE (blue). The solid lines represent the curves obtained by fitting of the data to the Nernst equation. The measurements were carried out in the presence of 40 μM Cyt *c* with 0 and 20% solutions of PEG, dissolved in 50 mM sodium phosphate buffer (pH 7.0) at 293 K.

**Figure 8**. **Proposed regulation mechanism of electron donation on Cyt *c* by specific dehydration around heme periphery.**

ACCEPTED MANUSCRIPT

ACCEPTED MANUSCRIPT

**Highlights**

- Reduced cytochrome *c* was rapidly oxidized in the presence of PEG.
- Heme oxidation was induced by a tertiary structural change with a slight shift in the heme position.
- PEG induces dehydration from Ile81 and Val83 of cytochrome *c*, which triggers the heme displacement.

ACCEPTED MANUSCRIPT

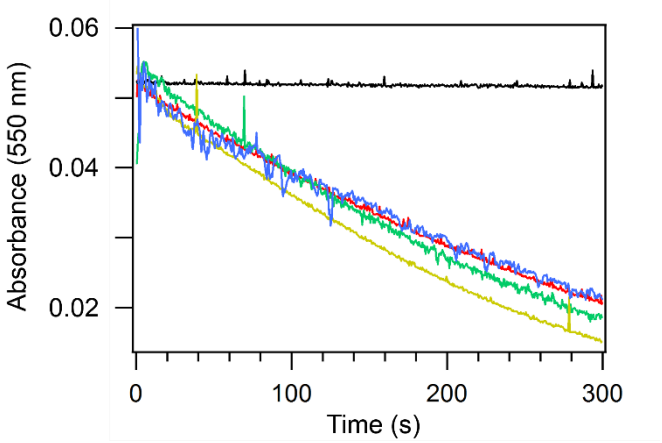


**Figure 1**. **Absorbance changes at 550 nm after addition of PEG 4000.** The measurements were performed by mixing of 3 μM ferrous Cyt *c* and 0 (black), 5 (red), 10 (yellow), 15 (green), and 20 (blue)% solutions of PEG, dissolved in 50 mM sodium phosphate buffer (pH 7.0) at 293 K under aerobic conditions.

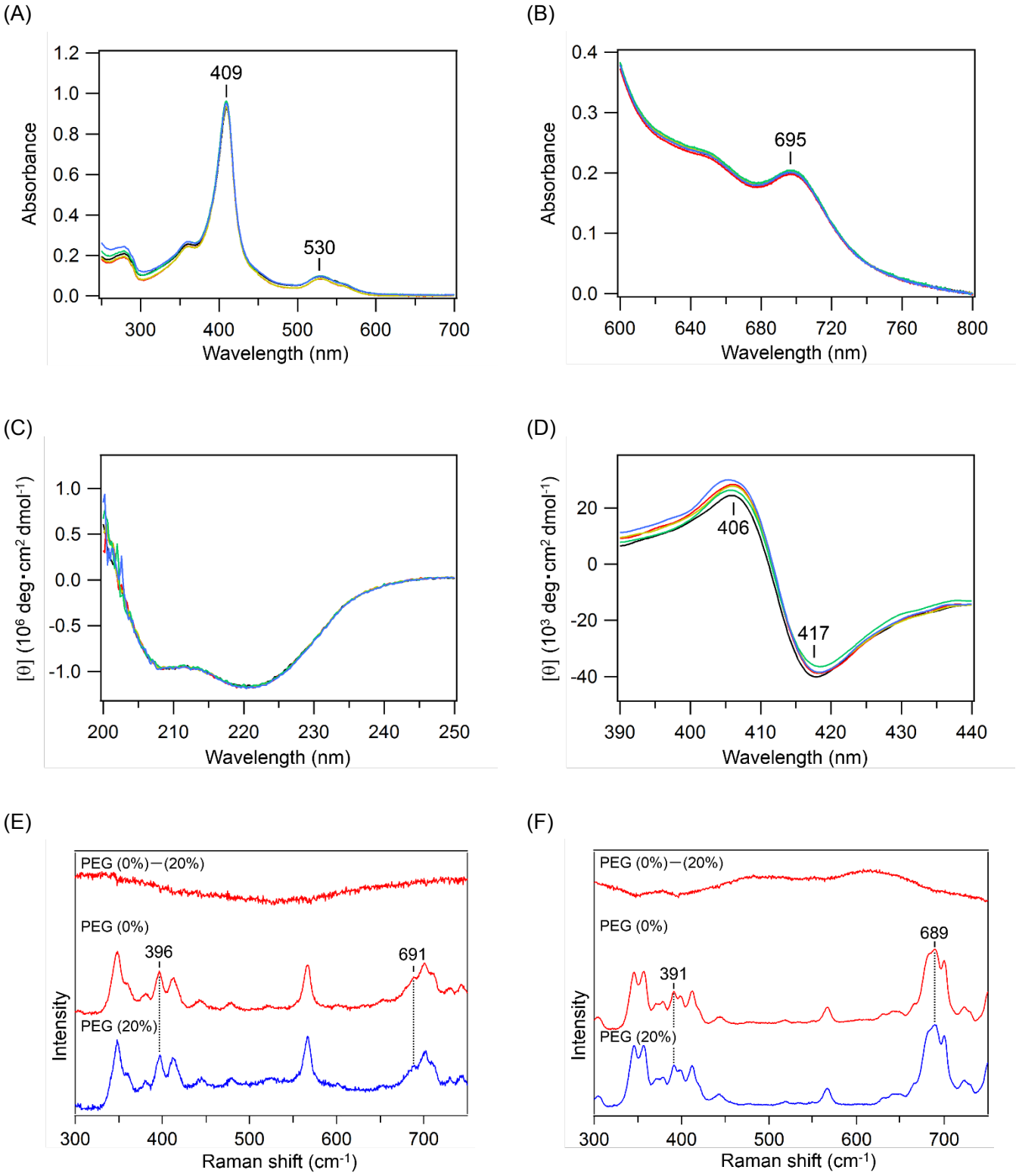


**Figure 2. UV-visible absorption, CD, and resonance Raman spectra of Cyt *c* in the presence of PEG.** Absorption spectra in the region between 250 and 700 nm of 8 μM oxidized Cyt *c* (A) and between 600 and 800 nm of 0.3 mM oxidized Cyt *c* (B). CD spectra in the far-UV region of 2 μM Cyt *c* (C) and in the Soret region of 10 μM Cyt *c* (D). These measurements were carried out in the presence of 0% (black), 5% (red), 10% (yellow), 15% (green), and 20% (blue) PEG. (E) (F) Resonance Raman spectra in the low frequency region of 50 μM oxidized (E) and reduced (F) Cyt *c*. These measurements were carried out in the presence of 0% (red) and 20% (blue) PEG. For all measurements, samples were dissolved in 50 mM sodium phosphate buffer (pH 7.0) at 293 K.

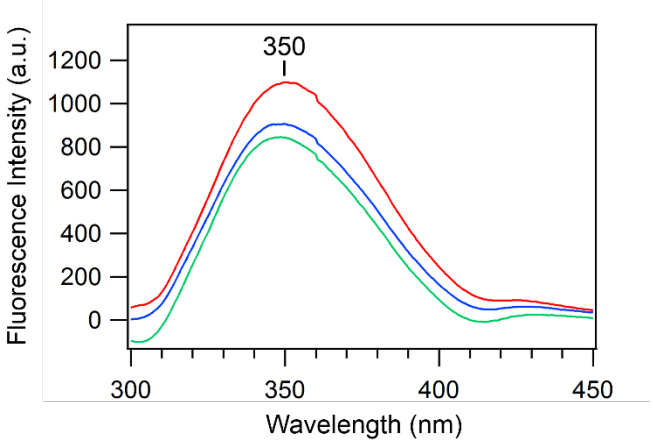


**Figure 3**. **Fluorescence spectra for the oxidized D2W mutant Cyt *c***. The measurements were carried out in the presence of 6 μM Cyt *c* with 0 (red), 10 (blue), and 20 (green)% solutions of PEG, dissolved in 50 mM sodium phosphate buffer (pH 7.0) at 293 K.

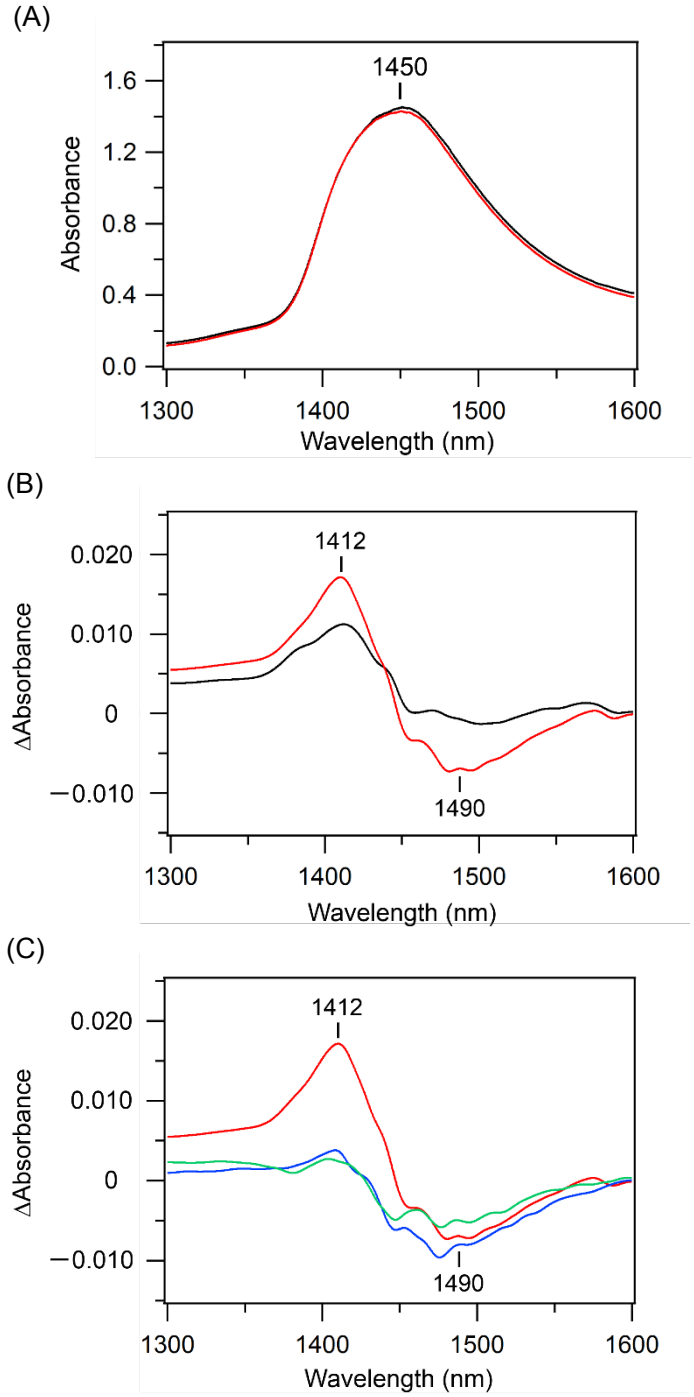


**Figure 4. NIR spectra of Cyt *c* in the region between 1300 and 1600 nm.** (A) NIR spectra in the absence (black) and presence of 50 μM Cyt *c* (red) dissolved in 50 mM sodium phosphate buffer (pH 7.0) at 293 K. (B) Difference NIR spectra subtracting the spectrum of buffer from that of 50 μM Cyt *c* (red) and that of 10 μM Cyt *c* (black). (C) Difference NIR spectra subtracting the spectra of buffer including 0 (red), 5 (blue), and 10% (green) PEG from that of 50 μM Cyt *c* in 0 (red), 5 (blue), and 10% (green) PEG solution.

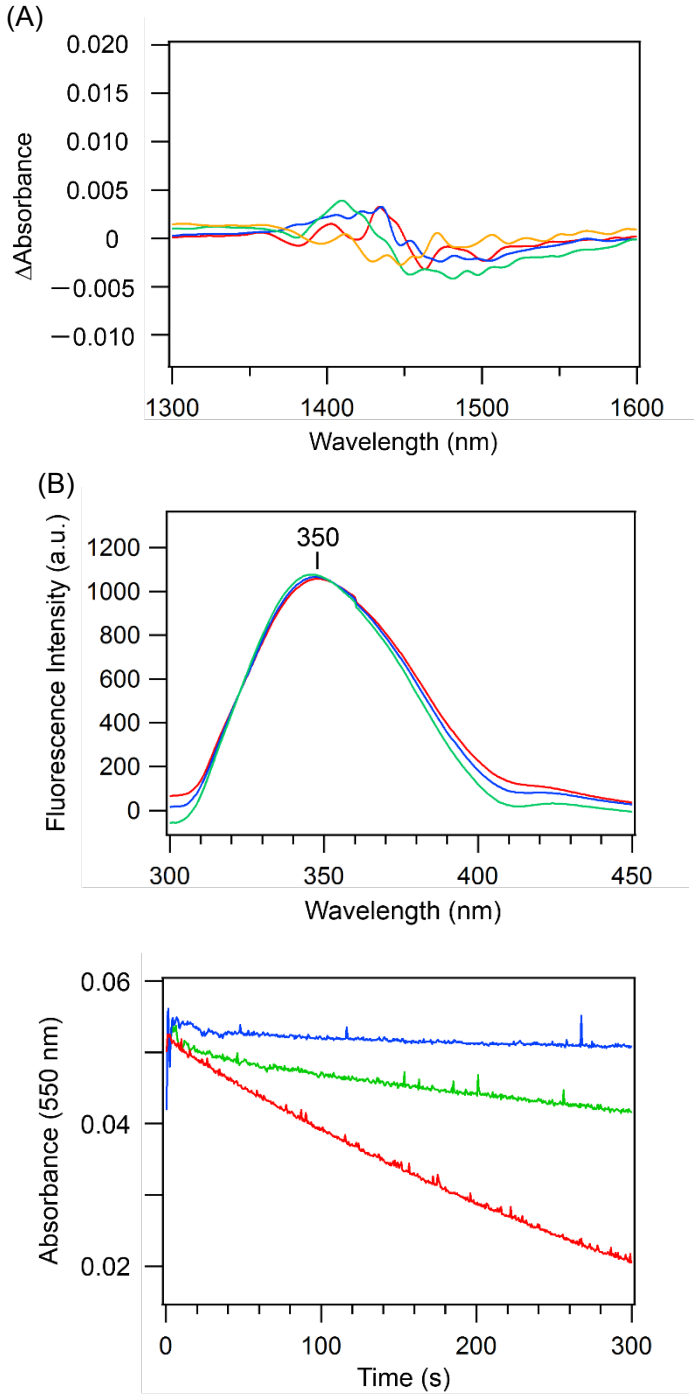


**Figure 5. Difference NIR spectra, fluorescence spectra, and absorbance change at 550 nm of mutants Cyt *c* in the presence of PEG.** (A) Difference NIR spectra subtracting the spectra of buffer including 0 (red), 5 (blue), and 10% (green) PEG from that of 50 μM V83S in buffer (orange) and I81S mutant Cyt *c* in 0 (red), 5 (blue), and 10% (green) PEG solution. The experimental conditions were the same as Figure 4C. (B) Fluorescence spectra for D2W/V83S mutant Cyt *c* in the presence of 0 (red), 10 (blue), and 20% (green) PEG. The experimental conditions were the same as Figure 3. (C) Absorbance changes at 550 nm of WT (red), I81S (blue), and V83S (green) Cyt *c* after addition of 5% PEG. The experimental conditions were the same as Figure 1.

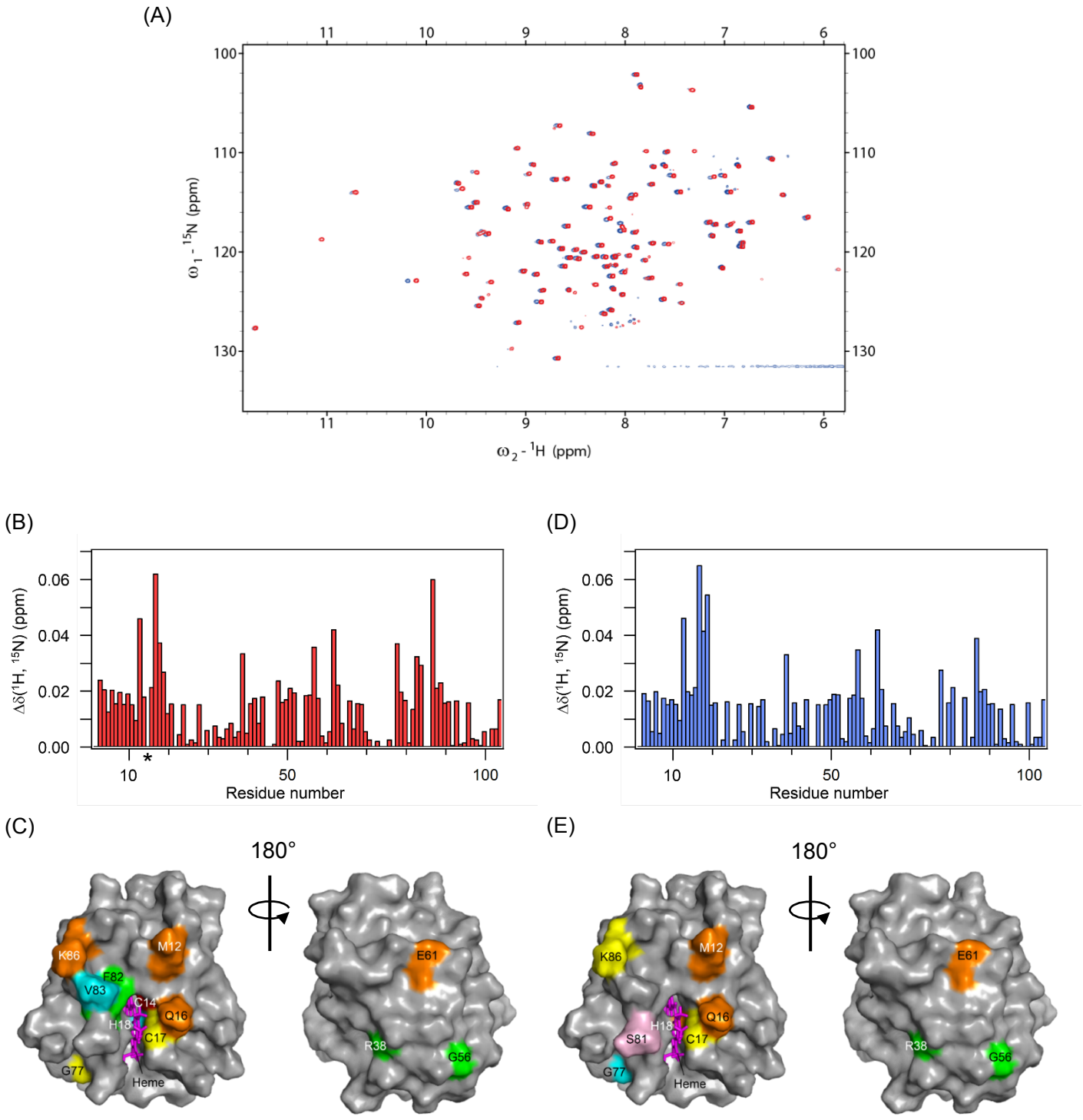


**Figure 6**. **Chemical shift perturbation in Cyt *c* in the presence of PEG.** (A) Superposition of the $^{1}$H-$^{15}$N HSQC spectra of $^{15}$N-labeled Cyt *c* in the absence (red) and presence of PEG (blue). Overview of the combined backbone chemical shift changes (bar graph) and line broadening (asterisk) of WT (B) and I81S mutant (D) Cyt *c* induced by addition of 20% PEG. Mapping of the affected residues on the surface of WT (C) and I81S mutant (E) Cyt *c*. The residues with chemical shift changes of $x \geq 0.042$, $0.042 > x \geq 0.037$, $0.037 > x \geq 0.032$, and $0.032 > x \geq 0.027$ are colored in orange, yellow, green, and cyan, respectively. In addition, red color represents the residues showing the specific line broadening. The measurements were carried out in the presence of 0.15 mM WT (B) or I81S (D) Cyt *c* with 0 and 20% solutions of PEG, dissolved in 50 mM sodium phosphate buffer (pH 7.0) at 293 K.

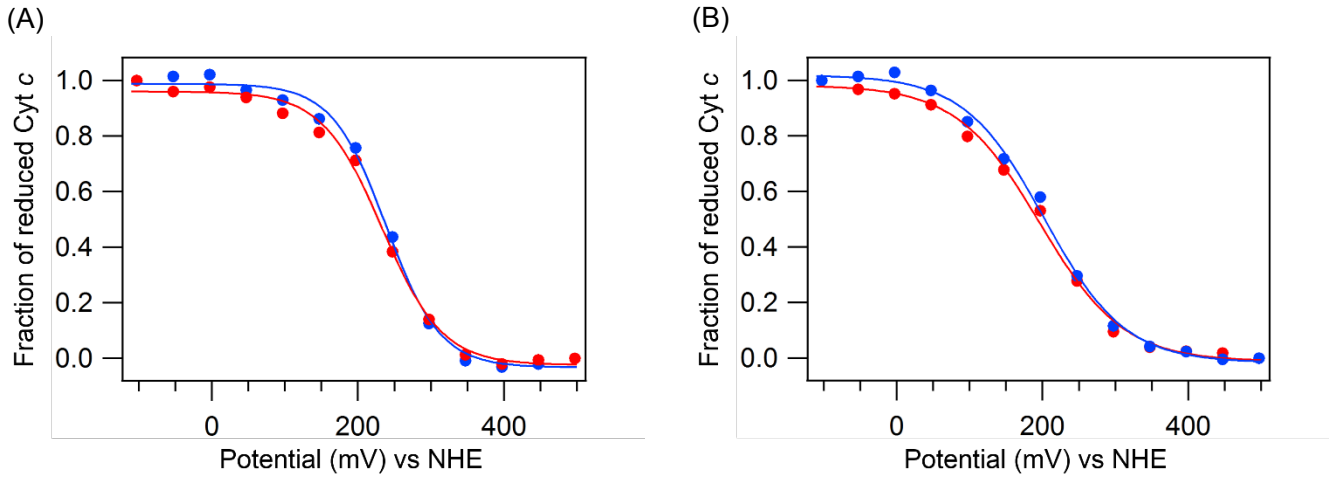


**Figure 7. Spectroelectrochemical redox titration of Cyt *c* in the (A) absence and (B) presence of 20% PEG.** The potential of electrode was decrease in 50 mV step from +500 to –100 mV vs NHE (red) and then increase from –100 to +500 mV vs NHE (blue). The solid lines represent the curves obtained by fitting of the data to the Nernst equation. The measurements were carried out in the presence of 40 μM Cyt *c* with 0 and 20% solutions of PEG, dissolved in 50 mM sodium phosphate buffer (pH 7.0) at 293 K.

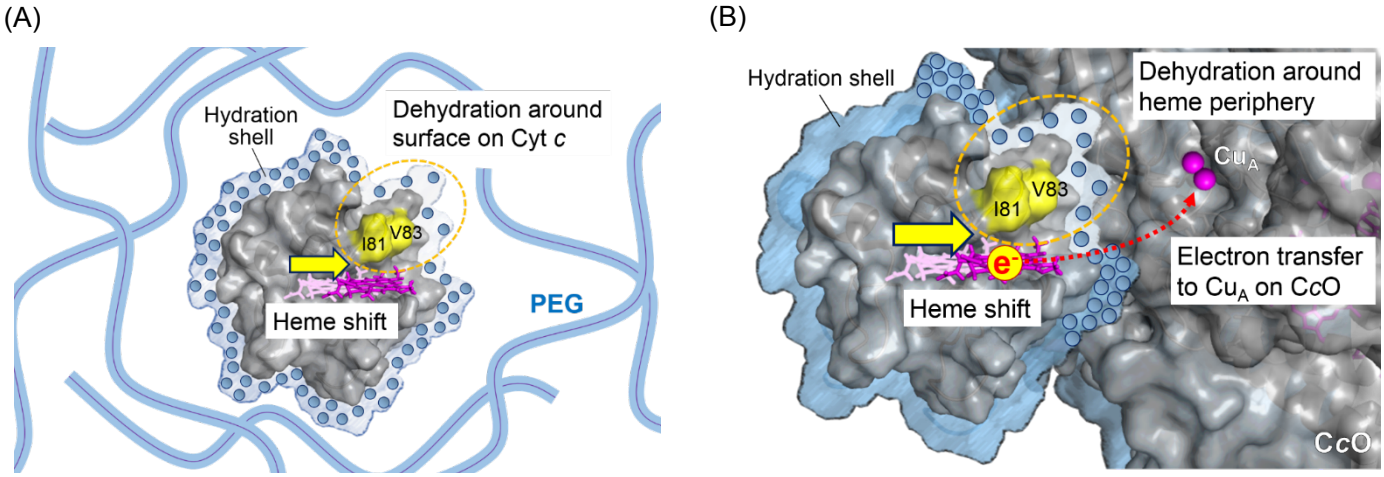


**Figure 8. Proposed regulation mechanism of electron donation on Cyt *c* by specific dehydration around heme periphery.**